J Therm Anal Calorim (2009) 98:655–666
DOI 10.1007/s10973-009-0516-3

Flow-induced crystallization regimes and rheology of isotactic polypropylene

Effects of molecular architecture

Juan F. Vega · Denka G. Hristova · Gerrit W. M. Peters

Rheological Analysis of Polymers/Special Chapter

Abstract We investigated the effect of flow in combination with molecular architecture on crystallization for linear and branched polypropylenes by means of dynamical mechanical spectroscopy. Compared to the linear polymer, the branched one exhibits much slower relaxation after deformation, causing higher levels of molecular orientation and molecular stretch for the same flow conditions. Different regimes of flow-induced crystallization are observed as a function of an increased level of molecular orientation and stretch. These regime changes cause the structure development in the material to vary from 3-dimensional spherulitical growth to nearly 1-dimensional fiber-like growth. Intermediate behavior is observed when the flow is strong (for the linear polymer) or weak enough (for the branched polymer), or in time when the effect of flow is exhausting. It is important to note that dynamical mechanical measurements can be used to probe different aspects of the (flow induced) crystallization process, such as a relative level of crystallinity and timescales of the evolution, but do not give absolute values. A correlation is found with the level of crystallinity obtained from real-time WAXS measurements and the kinetics of linear viscoelastic properties, but this correlation is not unique and depends on the pre-shear conditions applied.

J. F. Vega · D. G. Hristova · G. W. M. Peters (✉)
Dutch Polymer Institute, Eindhoven University of Technology, P.O. Box 513, 5600MB Eindhoven, The Netherlands
e-mail: g.w.m.peters@tue.nl

J. F. Vega
Departamento de Física Macromolecular, Instituto de Estructura de la Materia, CSIC, Serrano 113bis, 28006 Madrid, Spain

Keywords Linear and branched polypropylene · Crystallization · Dynamical mechanical spectroscopy · Crystallization regimes

Introduction

It is well known that the polymer molecular architecture, especially the topology (e.g., long chain branching, LCB) has a strong effect on melt rheological properties. Most of the studies concerns long-chain-branched-ethylene-based polyolefins as low-density polyethylene (LDPE) [1, 2] and metallocene catalyzed polyolefins [3–6]. These LCB polyolefins show extensive shear thinning, high elastic properties and extensional thickening, and also thermorheologically complex behavior. Nowadays it is possible to introduce LCB in isotactic polypropylene (iPP) by copolymerization [7, 8] These works account for some molecular, mechanical, rheological properties, and also for flow-induced crystallization (FIC) behavior monitored by small-angle X-ray scattering (SAXS) and wide-angle X-ray scattering (WAXS). It has been found that upon application of a step shear rate, the LCB-iPP materials show a higher fraction of oriented crystals and enhanced crystallization kinetics compared to linear iPP samples. Related features show a fibrillar and/or disk-like crystal growth morphology for these materials if strong flow is applied. The higher sensitivity of shear-induced crystallization for the branched material is thought to be caused by the broader relaxation time spectrum compared to the linear chain counterparts.

It is well known that flow gradients strongly affect the crystallization process, and, vice versa, the latter does affect the rheological behavior, i.e., the time evolution of the rheological properties of the material. Therefore, rheometry provides a complementary tool to study the structure

development during crystallization. One can expect, for example, differences in the evolution of viscoelastic properties for different morphological development processes [9]. Indeed, some authors concluded that rheological techniques are even more sensitive than the conventional ones to follow the crystallization process [10].

The aim of this work is, on one hand, to demonstrate the effect of shear flow on crystallization in combination with the molecular architecture and, on the other hand, to determine the different regimes as a function of the flow history. For that we apply short-term continuous shear on two different iPP's, a linear and a long chain branched one, and use small strain amplitude oscillatory measurements to track the crystallization process. The classification of the different regimes requires a full rheological characterization of the two polymers, something that is very often omitted in papers on FIC. Finally, we present some complementary results from X-ray scattering, giving direct access to structure development, and compare those to rheological results in order to demonstrate the complex relation between the real crystalline structure and the evolution of the rheological properties.

Experimental section

Materials

The rheological properties in the melt and their evolution during crystallization were measured on two different iPP samples. One is a linear polydisperse Ziegler–Natta iPP grade DSM15M10 (DSM, Geleen, The Netherlands), and the other a LCB-iPP, synthesized using a metallocene catalyst system (ExxonMobile) that contains a controlled amount of LCB. Molecular parameters and other physical properties (as far as available) of the materials studied are listed in Table 1. Basic rheological properties in the linear viscoelastic regime (from oscillatory shear measurements) have been obtained in the under-cooled melt at 418 K, by superposition of data obtained in the temperature range 418–523 K, using standard procedures. The results obtained for the temperature shift factors, a_T and b_T, WLF temperature coefficients, C_1 and C_2, (Maxwell) relaxation time distribution, $\{g_i, \tau_i\}$, Newtonian viscosity, η_0, and steady state compliance, J_e^0, are listed in Table 2 for both samples. In the temperature range explored, the application of the WLF equation to the shift factors, a_T, is equivalent to an Arrhenius temperature dependence, with values of the flow activation energy of $E_a = 39.6$ kJ mol^{-1} for the linear iPP and 49.9 kJ mol^{-1} for the branched iPP, in agreement with the values reported in the literature [11]. The results obtained in the LCB-iPP sample (higher temperature coefficients and elastic properties, together with a broader relaxation time distribution, despite a value of the Newtonian viscosity of the same order of magnitude than in the linear sample) are those expected in polyolefins with long chain branches [1–8]. This structural difference anticipates strong differences in molecular orientation and flow behavior.

Table 1 Molecular and physical parameters of the samples studied

Materials	M_w/g mol^{-1} [a]	M_w/M_n [a]	T_m/K [b]
Linear iPP	350000	5.6	434.0
LCB iPP	467000	3.6	427.4

[a] From size exclusion chromatography; [b] from differential scanning calorimetry

Flow-induced crystallization experiments

Rheology monitored flow-induced crystallization

Rheological experiments were conducted to monitor the isothermal crystallization kinetics at 418 K. The protocol followed is described below: (a) The samples were held at a temperature of 493 K for 10 min in order to remove any residual crystallinity before beginning the test; (b) the temperature was dropped to a value of $T_c = 418$ K at a cooling rate of -15 K min^{-1} and kept at this value. We have chosen this crystallization temperature after a preliminary study in the range 408–418 K (well below the T_m). At 418 K, the crystallization in quiescent conditions is slow enough in both polymers to allow the application of any mechanical history to the under cooled melt; (c) the time evolution of the elastic modulus G', the loss modulus G'', and the phase angle δ, were followed during the crystallization process. Oscillatory tests were conducted using an angular frequency of $\omega = 1$ rad s^{-1} and a strain of 0.005. Small sample sizes should be used to avoid transducer instabilities when the late stage of the crystallization process is achieved [12]. We used specimens with dimensions of 8 mm diameter, for which values of the moduli up to 10^8 could be measured without transducer instabilities. During thermal history, the gap was always compensated for to account for tool thermal changes.

For short-term FIC experiments, prior to (c) continuous shearing was applied during a shear time, t_s. The values of the shear rate applied varied from 2 to 100 s^{-1}, and the total strain from $\gamma = 60$–180.

Wide angle X-ray scattering

FIC was studied using time resolved WAXS. The experiments were performed at the ESRF in Grenoble beamline BM26 ($\lambda = 1.24$ Å, a linear gas detector was used for

Table 2 Rheological parameters at 418 K for the materials studied

LCB iPP			Linear iPP		
T/K	a_T/–	b_T/–	T/K	a_T/–	b_T/–
Shift factors					
418	1	1	418	1	1
433	0.55721	0.95238	433	0.62162	0.91528
448	0.40047	0.78163	448	0.40541	0.90507
463	0.24876	0.8	463	0.27027	0.896
478	0.14905	0.73159	478	0.20555	0.85568
493	0.10197	0.67283	493	0.15781	0.896
508	0.07575	0.51746	508	0.12751	0.82791
523	0.05719	0.43143	523	0.09662	0.77683
WLF					
C_1 [–]	4.619	–	C_1 [–]	2.754	–
C_2 [K]	287.7	–	C_2 [K]	180.5	–
Mode	g_i 10^{-4}/Pa	τ_i/s	Mode	g_i 10^{-4}/Pa	τ_i/s
Maxwell modes					
1	7.77	0.004	1	8.86	0.008
2	3.67	0.023	2	3.93	0.052
3	1.81	0.14	3	1.85	0.34
4	0.420	0.78	4	0.519	2.21
5	0.150	4.56	5	0.0811	14.4
6	0.0260	26.5	6	0.0092	93.5
7	0.004	154	7	–	–
8	0.0008	893	8	–	–

Properties			
η_0 10^{-3}/Pa s	J_e^0/Pa^{-1}	η_0 10^{-3}/Pa s	J_e^0/Pa^{-1}
33.0	0.027	43.5	0.0021

Relaxation times/s:	LCB iPP ($Z = 90$)				Linear iPP ($Z = 70$, $Z_{HMW} = 2300$)					
	$\bar{\tau}_d$	τ_R	τ_d^{long}	τ_R^{long}	$\bar{\tau}_d$	τ_R	τ_d^{long}	τ_R^{long}	τ_d^{HMW}	τ_R^{HMW}
	117.0	0.433	893	3.31	24.5	0.116	93.5	0.446	5720	0.870
$\dot{\gamma}_{I\to II}$/s^{-1}	8.55×10^{-3}	–	1.12×10^{-3}	–	0.041	–	0.011	–	1.7×10^{-4}	–
$\dot{\gamma}_{II\to III}$/s^{-1}	–	2.31	–	0.30	–	8.60		2.24	–	1.15

Time–temperature shift factors for WLF fit, C_1 and C_2; Maxwell model modes parameters, g_i and τ_i; rheological basic parameters, η_0, and J_e^0; Maxwell model averaged relaxation time, $\bar{\tau}_d$, Maxwell model longest relaxation time, τ_d^{long}; and the corresponding Rouse relaxation times from Eq. 1, τ_R and τ_R^{long}; characteristic relaxation time of the high-M_w tail of the molecular weight distribution, τ_d^{HMW}, estimated from molecular theory (Eq. 2), and the corresponding Rouse relaxation times from Eq. 3, τ_R^{HMW}; critical values of the shear rate for the transitions between regimes I and II ($\dot{\gamma}_{I\to II}$) and regimes II and III ($\dot{\gamma}_{II\to III}$)

WAXS experiments). The time interval between the X-ray patterns was varied from 3 s at the beginning at the process to 15 s at the late stages of crystallization. In this way the beginning of the crystallization was followed as precisely as possible because most of the changes in the structure happen during the early stages of the process. A Linkam shear cell device was used to apply well defined thermo-mechanical history to the polymer melts. Sample geometry is the same than in rheological experiments, and then a similar shear history is expected. A sample with the shape of a disk with a thickness in the range of 500 to 800 μm was inserted and the same time–temperature protocol as for rheological measurement was used for all shear experiments. Shear experiments were performed for different shear times and for a total shear strain of from $\gamma = 60$ to 180 at a temperature of $T_c = 418$ K.

Results

Flow-induced crystallization monitored by rheology and WAXS

Continuous flow

In Fig. 1a, b the transient experiments results at $T_c = 418$ K are presented for both materials and for shear rates of 0.1, 4, and 60 s^{-1}. For all experiments a steady-state period is observed before an increase in the viscosity function sets in as a consequence of the onset of the crystallization process. For the smaller shear rates the onset of the crystallization takes place at much longer times for the linear iPP (Fig. 1a). However, for the shear rate of 60 s^{-1}, a similar onset time is observed for both linear and branched materials. We have to point out here that the effect of the flow on the branched material is much stronger (Fig. 1b), even taken into account that the degree of undercooling is lower for this material (the melting temperature is 7° lower than for linear sample).

Defining a characteristic time for the crystallization rate by taking the time at which the upswing in the viscosity

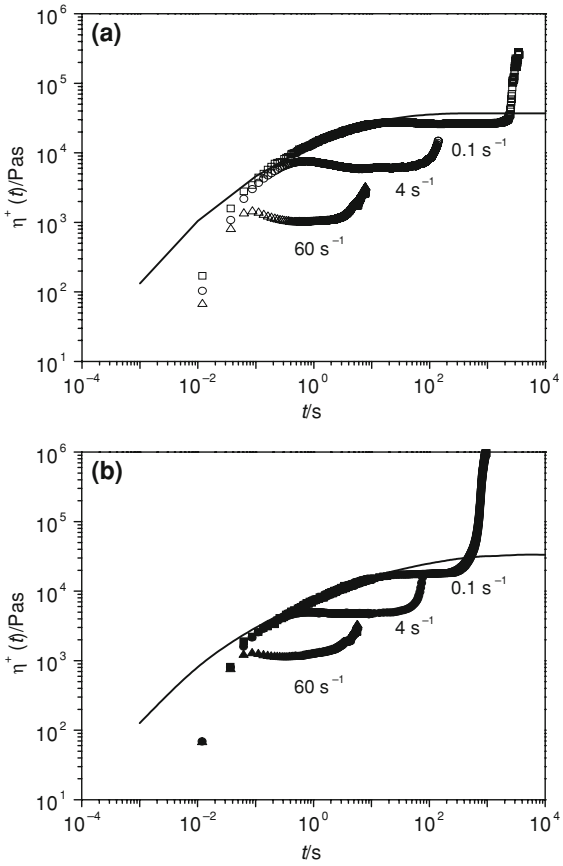

Fig. 1 Transient shear viscosity at 418 K and different shear rates for the materials studied **a** linear iPP and **b** branched iPP

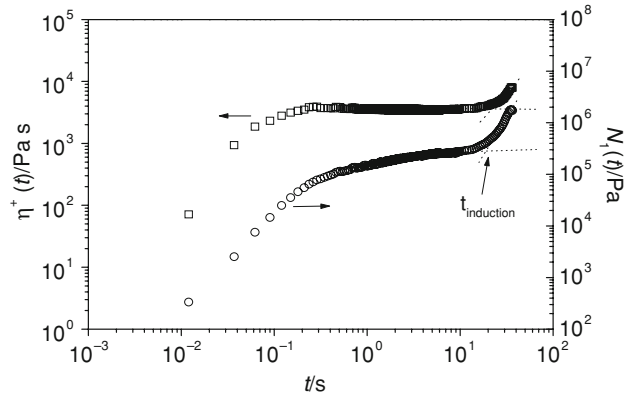

Fig. 2 Time evolution of the viscosity (*square*) and the first normal stress difference (*circle*) for the linear iPP at 418 K and $\dot{\gamma} = 10\,s^{-1}$

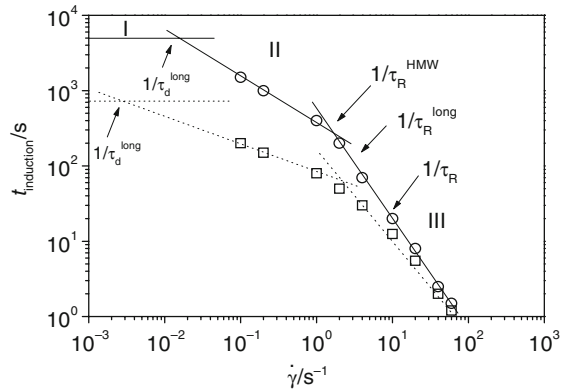

Fig. 3 Dependence of the induction time of the flow enhanced crystallization process for the linear (*circle*) and the branched (*square*) iPPs at 418 K in continuous shear. The *arrows* indicate the magnitude of the critical shear rate values for the orientational crystallization ($1/\tau_d$) and stretching crystallization ($1/\tau_R$) obtained from the different approaches for the linear iPP. *Horizontal lines* indicate the value of the induction time for quiescent crystallization

and first normal stress difference coefficient curves occur for FIC (see Fig. 2 for a graphical definition), the influence of flow rate can be classified. The results are given in Fig. 3. The main observation is that there are two different regimes of crystallization enhancement. The transition between these regimes is most clear for the linear iPP. This result shows how rheology can be used to investigate the influence of flow on crystallization and to reveal, for example, different regimes that depend on flow strength.

Short-term experiments

For these series of experiments the influence of the flow rate, the shear stress level reached, and the shear time has been studied within the different FIC regimes identified in Fig. 3. In Fig. 4a, b the results of the evolution of the

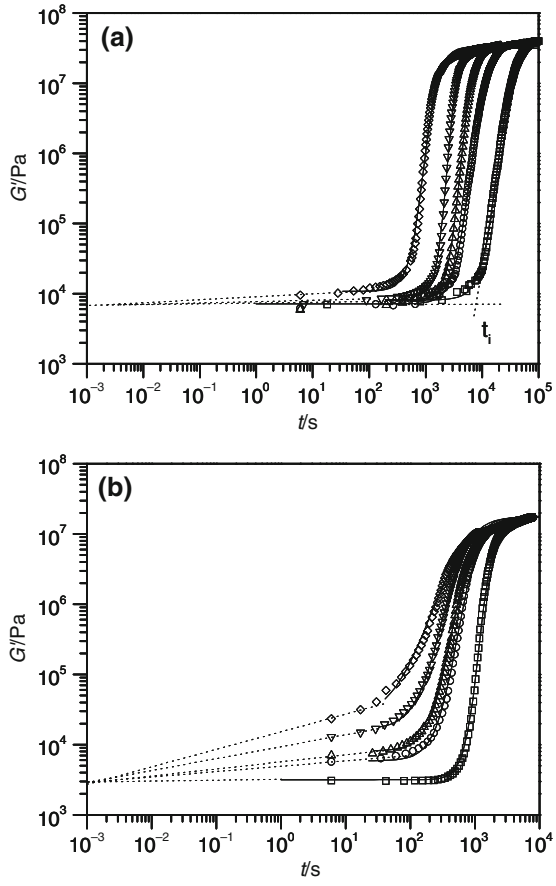

Fig. 4 **a** Time build-up of storage modulus for linear iPP at 418 K for quiescent conditions (*square*) and after different pre-shear conditions for $\gamma = 60$: (*circle*) 4 s^{-1} for 15 s, (*triangle*) 10 s^{-1} for 6 s, (*inverted triangle*) 40 s^{-1} for 1.5 s, and (*diamond*) 60 s^{-1} for 1 s. **b** The same results are observed for branched iPP sample. The *dashed lines* are drawn to guide the eye

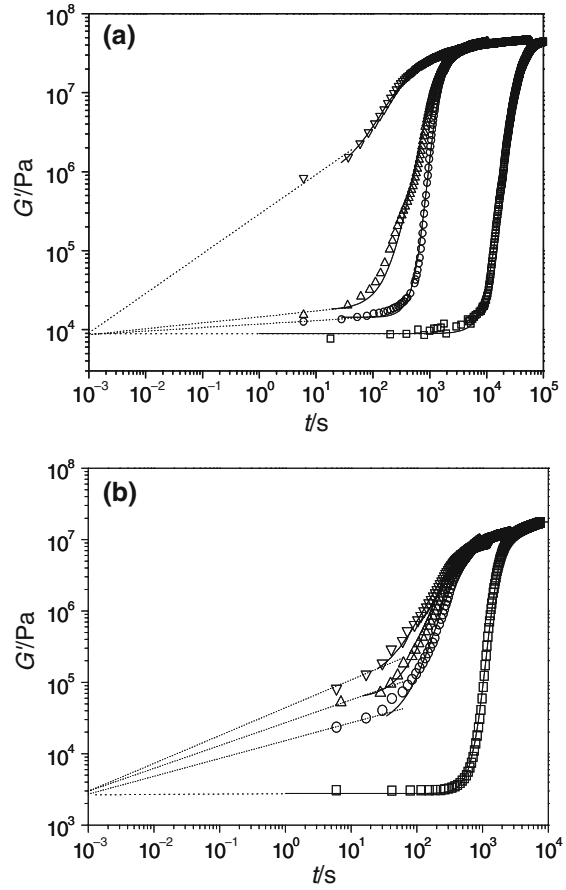

Fig. 5 **a** Time build-up of storage modulus for linear iPP at 418 K for quiescent conditions (*square*) and after different pre-shear conditions for a shear rate of 60 s^{-1}: (*circle*) shear time 1 s, (*triangle*) shear time 2 s, and (*inverted triangle*) shear time 3 s. **b** The same results are observed for the branched iPP sample. The *dashed lines* are drawn to guide the eye

storage modulus G' at temperature of 418 K for quiescent and FIC for a total strain $\gamma = 60$, and increasing shear rate (from 4 to 60 s^{-1}) are presented for the linear and the branched materials. All the data correspond to experimental times taken after cessation of flow. The important observations that can be made from these results are: (a) for the linear iPP only an effect in the time for the onset of the crystallization is observed. On the contrary, for the branched iPP important changes in the initial value of G' (higher than the corresponding for the undercooled quiescent melt) are observed even for a pre-shear condition of 4 s^{-1}; (b) the evolution of the kinetics process (the slope of the curves) seems not to be affected by the shear rate in the linear iPP (Fig. 4a), at least up to the level of total strain reached in these experiments ($\gamma = 60$), i.e., the slope for the time dependence of the crystallization process is a constant. However, for the branched sample a gradual change in the process is observed (Fig. 4b). Recently, the evolution of viscoelastic properties during crystallization of the linear iPP sample has been successfully modeled by using a suspension-based rheological model, at least for these low-strain levels [13].

The effect of higher strain levels has been also explored. In Fig. 5a, b the results for crystallization process are observed for constant shear rate of 60 s^{-1} and increasing shear time of 1, 2, and 3 s, respectively. As in Fig. 4a, b, all the data correspond to experimental times taken after cessation of flow, but a clear difference is observed when the results are compared. The branched polymer, again, shows smoothly changing kinetics. However, the kinetics in the linear sample shows a sudden change for the higher shear times. For 3 s the time dependence of rheological properties becomes even similar to that observed in the branched sample for the same conditions. Defining a flow enhancement crystallization parameter, the crystallization half time, θ, by taking the ratio of the times at which the half change in the viscoelastic functions occurs for

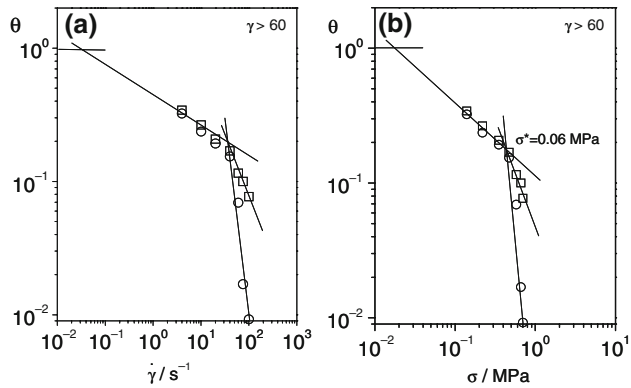

Fig. 6 Enhanced crystallization half-time factor, θ, obtained from dynamical mechanical experiments for the linear (*circle*) and the branched (*square*) iPPs versus shear rate (**a**) and shear stress (**b**) applied during the pre-shear condition for shearing times of τ_s = 1–15 s ($\gamma \geq 60$)

quiescent and FIC (from Figs. 4 and 5) with respect to the quiescent melt horizontal line, the influence of flow rate and shear stress can be quantified. The effect of shear rate and shear stress on θ is given in Fig. 6. Once again a transition is observed above a critical shear rate/shear stress value, but now for both polymers this transition is rather sharp.

The results obtained in the WAXS experiments can be observed in Figs. 7, 8, 9. In Fig. 7 the 2D WAXS patterns are also shown for three different flow conditions (quiescent, and $\dot{\gamma} = 60\,s^{-1}$ with $t_s = 1$ and 3 s) in the case of the linear iPP sample. Figure 8 gives the crystallinity as a function of time for the linear and branched samples for quiescent and the two flow conditions $\dot{\gamma} = 60\,s^{-1}$ and $t_s = 1$ and 3 s. Again, the enhancing effect of flow on the crystallization rate is observed, following the same trends obtained in rheological measurements. In fact, as we will be shown later in more detail, the time scale for the onset of crystallization is nearly the same if the time evolution of crystallinity measured by WAXS is compared with the fractional change of viscoelastic properties. In Fig. 9, G' values obtained from rheological measurements for which the same conditions were used, is plotted as a function of the crystallinity obtained from WAXS. The first important thing to notice is that there is no unique relation between the modulus and crystallinity; depending on the flow conditions different values of G' can be found for the same level of crystallinity in both polymers. This implies the reverse way, i.e., using G' as a measure of the crystallinity (a very often used assumption) is not an option. Nevertheless, we still use in the sequel of this paper the Avrami analysis of the rheological properties to distinguish between different regimes of structure in terms of the rate and type of geometrical changes of the growing structures.

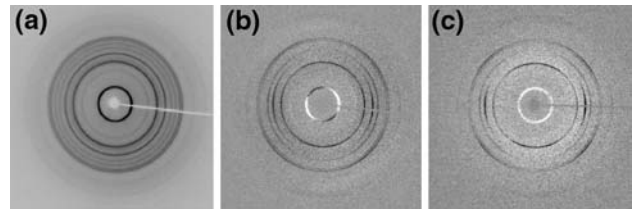

Fig. 7 WAXS patterns for the linear iPP: **a** quiescent case, **b** 60 s^{-1}/1 s, **c** 60 s^{-1}/3 s

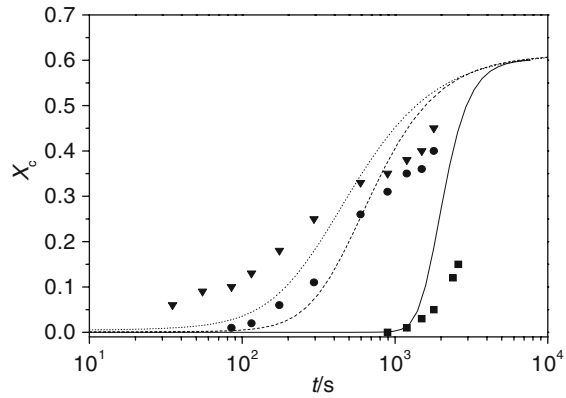

Fig. 8 Time evolution of crystal fraction obtained by 2D-WAXS, X_c (*symbols*), and the calculated from transformed fraction a using viscoelastic measurements (*lines*) under different pre-shear conditions for branched iPP. (*square*) Quiescent, (*circle*) 60 s^{-1}/1 s, and (*inverted triangle*) 60 s^{-1}/3 s. The (*lines*) correspond to the results obtained by the application of Eq. 5 to the experimental results for quiescent (*solid line*); 60 s^{-1}/1 s of pre-shear (*dashed line*); and 60 s^{-1}/3 s of pre-shear (*dotted line*)

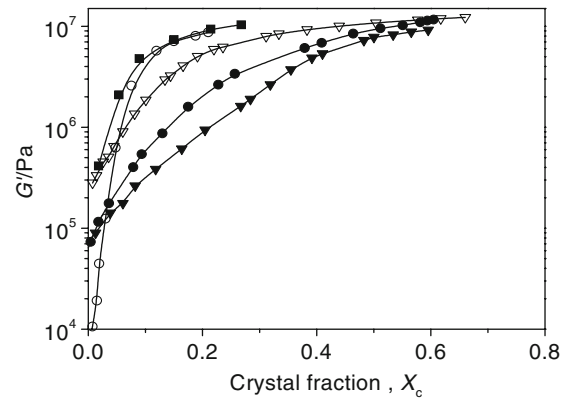

Fig. 9 Storage modulus (from rheology) versus crystal fraction obtained by 2D-WAXS in linear iPP (*open symbols*) and branched iPP (*solid symbols*) under different pre-shear conditions: branched iPP: (*filled square*) quiescent, (*filled circle*) 60 s^{-1}/1 s, and (*filled inverted triangle*) 60 s^{-1}/3 s; linear iPP: (*open circle*) 60 s^{-1}/1 s and (*open inverted triangle*) 60 s^{-1}/3 s

Discussion

Continuous shear flow: classification of regimes

There are two characteristic times that define two different regimes for the FIC [14, 15]. For values of the shear rate higher than $1/\tau_d$, τ_d being the reptation or disengagement time, but lower than $1/\tau_R$, τ_R being the Rouse time, only orientational effects on (point) nucleation takes place. The critical Deborah number for this regime is defined as $De_0 = \tau_d\dot{\gamma} = 1$. However, for values of the shear rate higher than $1/\tau_R$, molecular stretching occurs giving rise to a fibrillar morphology development in crystallization [16, 17]. In this case the critical Deborah number is defined as $De_s = \tau_R\dot{\gamma} = 1$. From our rheological data in the melt (using the temperature shift factors in Table 2), represented by a discrete spectrum of Maxwell modes, we obtain the average reptation time $\bar{\tau}_d$ and the longest reptation time, τ_d^{long}, in the under-cooled melt (418 K). For these two reptation times the corresponding values of τ_R can be estimated according to the relationship [18]:

$$\tau_R = \frac{\tau_d}{3Z} \tag{1}$$

where Z is the average number of entanglement defined as $Z = M_w/M_e$. The values obtained from GPC are $Z = 70$ for the linear sample and $Z = 90$ for the branched one, with $M_e = 5200$ g mol^{-1} for iPP [19]. The results of calculating the characteristic shear rate values for the orientational and fibrillar regimes from $\bar{\tau}_d$ and τ_d^{long} and the corresponding $\bar{\tau}_R$ and τ_R^{long} (obtained from Eq. 1) are summarized in Table 2. The orientational regime starts for critical shear rate values of $\dot{\gamma} = 0.001$–0.01 s^{-1}. For the fibrillar regime a 1–2 order of magnitude higher shear rate value is required. The rheological relaxation times have no a direct connection with the MWD and thus are not useful to investigate the role of the high molecular weight tail of the MWD. However, for the linear iPP it is possible to estimate the corresponding relaxation times of the HMW species of the MWD, τ_d^{HMW} and τ_R^{HMW}. The linear iPP has a value of $Z_{HMW} = 2300$ [14]. From the framework of the widely accepted reptation theory applied to polymer dynamics [18], these characteristic times, for a monodisperse linear polymer, depend mainly on chain length (or the number of entanglements, Z), expressed by the following expressions [20]:

$$\tau_d = 3\tau_e Z^3\left[1 - \kappa\left(\frac{1}{Z}\right)^{0.5}\right]^2 \tag{2}$$

$$\tau_R = \tau_e Z^2 \tag{3}$$

where τ_e is the equilibration time of an entanglement segment and κ is a constant of the order of unity ($\kappa = 1.51$) [21]. The calculation of these characteristic relaxation times requires the knowledge of τ_e for iPP. An estimation of this value can be obtained from the monomeric friction coefficient, ζ_0, and other material physical constants, by means of the expression:

$$\tau_e = \frac{\zeta_0 \frac{\langle R^2\rangle}{M} M_e^2}{3\pi^2 k_B T m_0} \tag{4}$$

where $\langle R^2\rangle/M$ is the monodisperse chain end-to-end distance molecular weight ratio for an ideal equilibrium random coil, M_e the average molecular weight between topological constraints, m_0 the molecular weight of the monomeric unit, k_B the Boltzmann constant, and T is the absolute temperature. The values of $\langle R^2\rangle/M$ and M_e can be found in the literature [22, 23]. The monomeric friction coefficient has been recently obtained from linear viscoelastic results of metallocene-catalyzed iPPs (with narrow molecular weight distribution) at a temperature of 463 K [19]. Using the temperature shift coefficients in Table 2, and the material physical constants in Table 3, we found τ_e to be 1.64×10^{-7} s at 418 K. Following this approach for the linear iPP, the results for the characteristic shear rate values for the orientational and fibrillar regimes based on the HMW tail are calculated and given in Table 2. It is important to notice that, in this case, the value obtained for $\dot{\gamma}$ is remarkably close to the experimental transition between the two-flow-induced crystallization regimes (see Fig. 3). Figure 3 shows three different regimes of crystallization enhancement. Regime I ($\dot{\gamma} < 1/\tau_d^{\text{long or HMW}}$), i.e., no influence of flow, is given by a horizontal line that was obtained from induction time for quiescent crystallization experiments (Fig. 4a, b). The onset of the other two flow influence regimes can be captured with two characteristic times that relate to each other as the reptation time to the Rouse time (chain stretch relaxation time). Regime II, the chain orientation regime, is the regime for which a mild influence of the flow is seen ($\dot{\gamma} > 1/\tau_d^{\text{long or HMW}}$, $\dot{\gamma} < 1/\tau_R^{HMW}$) related to flow-induced homogeneous point nucleation and, finally, regime III in which the

Table 3 Physical constants for isotactic polypropylene at 463 K

Material	$\langle R^2\rangle/M$/Å^2 g^{-1} mol [22, 23]	m_0/g mol^{-1}	G_N^0/MPa [22, 23]	M_e/g mol^{-1} [a]	ζ_0/kg s^{-1} [16]
iPP	0.694	42	0.45	5200	2.3×10^{-12}

[a] Calculated from $M_e = 4\rho RT/5G_N^0$ at 463 K

influence of the flow is much stronger ($\dot{\gamma} > 1/\tau_d^{\text{long or HMW}}$, $\dot{\gamma} > 1/\tau_R^{\text{HMW}}$) leading to the occurrence of fibrillar nuclei and, from that, shish-kebab structures. This is in quantitative agreement with the classification given by van Meerveld et al. [14], who defined four regimes. We do not observe the intermediate regime. This intermediate regime was defined for strong enough flow ($\dot{\gamma} > 1/\tau_R$) but a too short shear time to reach a *critical molecular stretch* that could cause rotational isomerization of the chain (i.e., a non-Gaussian configuration), leading to fibrillar structures. Again, notice that all this is based on reptation and onset of chain stretch of the high molecular weight tail. This is all true for the linear iPP; for the branched iPP we have to interpret this numbers as equivalent numbers. This case is more complex, because it is not possible to apply the approach given by Eqs. 1–3, developed for flexible, linear polymers. What we can say in this case is that the transition between orientational and fibrillar regimes is more ambiguous. The molecular architecture of branched polymers is rather complex. These materials are usually composed of very different kinds of molecular species, with no constant amount and/or frequency of branches along the backbone. This means that the degree of orientation can vary depending on the molecular specie, which then gives rise to a hazy distribution of orientational effects due to the flow. This provokes the transition between the different regimes to be less sharp compared to the linear polymer as it is clearly observed in Fig. 3. However, by drawing lines through the induction quiescent time and the first four and last three points, an orientational transition point can be defined that is approximately shifted a decade and this is about the same ratio as found between the reptation times (see Table 2). For the transition to regime III a similar order of magnitude than for the linear iPP has been found.

Returning to the intermediate regime, which is part of the stretching regime ($De_s > 1$), van Meerveld el al. [14] have defined two different cases. For small chain extension ratio, λ, the chains maintain a Gaussian configuration, but at large λ, the influence of finite extensibility of the chain sets in, rotational isomerization occurs and the chain configuration becomes non-Gaussian. A critical value λ^* identifies the transition between these weak and strong stretching conditions. Crystallization occurs in this case following a 1-dimensional growth of the crystals. We cannot extract any conclusion about the existence of this regime from the results in Fig. 3, because no change in the slope is observed. However, it is very possible that the HMW chains present in the polymers studied fulfill the condition $\lambda > \lambda^*$ as the chains are subjected to strong flow conditions for a sufficiently long time. We will explore this in the next section.

Short time shear: the stretching regime

From the above it follows that a certain level of the shear rate is required to observe the enhanced rheological properties due to FIC. We will discuss now the results obtained of the rheological monitoring of FIC at different pre-shear conditions, reaching different and specific levels of total shear strain (applying shear rate higher than $1/\tau_R^{\text{HMW}}$) prior to the dynamic time sweep. From Figs. 4 and 5 the following can be observed:

(a) In Fig. 4a, b (experiments with a pre-shear condition with total shear strain $\gamma = 60$) no initial or a very small change in G' is observed for the linear sample. Moreover the same kinetics for the build-up of G' is observed. For the branched sample a different time evolution of viscoelastic properties is obtained, depending on the pre-shear condition applied. Not only an enhanced crystallization kinetics (lower values of the induction time as shear rate increases) is obtained, but also a considerable increase of the initial value of G' and changes in the time dependency of the viscoelastic properties. This occurs for the branched polymer even for the lowest shear rate value.

(b) From Fig. 5a, b (experiments with increasing total shear from 60 to 180) a clear increase in G' is observed from the beginning of the experiments, pointing to the existence of some initial structure in the "melt." However this occurs for the linear sample only if the flow is strong, i.e., 60 s^{-1}, and if this shear rate is applied for a long enough shear time (i.e., 3 s). This means that the effect of branching is the same as for a strong shear applied to a linear polymer.

As the viscoelastic response of a material is directly related with structure, we can argue that the changes observed are due to different morphologies developing and different kinetics in the under cooled melt, which give rise to a different increase of the viscoelastic properties. Moreover, the initial high values of the linear viscoelastic properties indicate that the morphology emerges in a very short time, i.e., in less than 5 s, the time required for the first point of the dynamic experiment after flow cessation (see dotted lines in Figs. 4 and 5). In these cases the calculation of θ requires the extrapolation to very short times. As it can be observed in Figs. 4 and 5, the trends given by the dotted lines suggest that the linear viscoelastic properties start to grow instantaneously (10^{-3} s).

From Fig. 6a the different stretch regimes, as classified by van Meerveld et al. [14] are again observed. Now the plot corresponds to the flow enhancement crystallization parameter, θ, defined previously, for the experiments that

fulfill the condition $\gamma > 60$. A transition is found at a critical shear rate of approximately 30–40 s^{-1} corresponding to a value of the shear stress of around 0.06 MPa (see Fig. 6b). With the Rouse time $\tau_R^{HMW} = 0.87$ s for the linear iPP (see Table 2), the corresponding De_s number is approximately 35. This corresponds rather well with the values presented by van Meerveld et al. [14] for similar conditions and when applying the same method, i.e., estimating τ_R from the high molecular weight part of the MWD. They presented values for $De_s = 0.6$–20 for experiments performed at 413 K (see Table 1 in that paper). At a higher temperature a little higher De_s is expected (see also Table 1, cases 20, 24, and 28 in that paper). As we do not know the molecular stretch and, moreover, no unique universal value for the critical strain is given by van Meerveld et al. [14] we use the macroscopic shear strain as measure for estimating the critical level of stretch that sets the transition between the two regimes. For all the cases in Fig. 6 the strain is approximately $\gamma = 60$. For the HMW molecules (large relaxation time) and such a large value of the macroscopic strain, this could be a good estimate for the molecular strain. Using results from extensional experiments as found in literature [24, 25], van Meerveld et al. [14] estimated critical strain levels for the HMW strain stretch to be of the order of 10. This is, again, of the same order and, considering the crude approximations, in reasonable agreement with our estimated stretch level. However, all the experiments performed have reached this macroscopic strain level, but only those for which $\sigma > 0.06$ MPa show a clear transition in what θ values concerns (see Fig. 6b).

Returning to the case of a constant continuous shear rate and varying shear times experiments (Figs. 1 and 2), and again restricting to the linear polymer, we can also estimate the critical macroscopic strain that is required to change from one regime to the other (see Fig. 3). For a shear rate of 1.2 s^{-1}, using the induction time $t_{induction} = 400$ s, this now found to be in the order of $\gamma = 500$. For increasing shear rates the strain at which the solidification of the polymer sets in decreases; for the critical shear rate of 40 s^{-1} it is found to be in the order of $\gamma = 80$ ($t_{induction} = 2$ s). The latter difference with the value found from short-term experiments is due to the definitions of the characteristic times (induction time versus half crystallization time). The transition of the regimes for continuous flow taking place at a much lower shear rate and the differences in strain for different shear rates is due to the ongoing flow enhanced (point) nucleation. The nuclei form physical cross-links that are changing the rheological behavior of the melt, in particular the relaxation spectrum and, more specific, the largest relaxation time corresponding to the HMW molecules as these are molecules that were (first of all) involved in the flow enhanced nucleation process (see Zuidema et al. [26] where the idea of the cross-linking melt was used). This implies that the *De* is increasing in time and, after sufficient cross-linking has taken place, the critical De_s is reached and regime III sets in. Of course, this process is in competition with the crystallization process itself (growth of the crystals), which can also cause the upswing in the viscosity before the critical De_s is reached. This clearly happens for low continuous shear rate experiments, for which the regime II is detected.

With respect to the branched polymer the following remarks can be made. First of all, the relaxation time of the molecular parts between the branches, especially the most "internal" parts, is much larger than that of the highest relaxation times of the linear polymer (see also the spectra in Table 2). However, the transition between the regimes seems to take place at similar shear rate, i.e., at a much higher De_s when defined with the highest value of the spectrum. It seems that in the first part there is no influence of the LCB; the slope of curves is nearly the same, as it is seen in Fig. 6. However, once the transition takes place the slope of the change of viscoelastic properties is different. When, for this case, the crystallization half time is plotted versus the applied (total) shear stress (Fig. 6) we can observe that a change in the regime occurs when a critical shear rate stress $\sigma^* = 0.06$ MPa is reached in both linear and branched iPPs. It is remarkable that the value of σ^* is the same as that found by Seki et al. [27] who also studied the flow-induced crystallization of iPP.

We can make however further considerations about the results shown in Figs. 4, 5, 6. When the shear is above the critical value, G' is already considerably changed when the first value is measured (6 s after the applied shear flow was stopped). For a shear rate of 60 s^{-1} and a shear time of 3 s this is even two decades (see Fig. 5a). Therefore, the use of the crystallization halftime for these cases can be questioned. Comparing the characteristic times of the two materials in Table 2, as far as possible, typically those of the branched iPP are a decade larger. Assuming that the critical values for the *De* number are the same for both materials implies that critical shear rates for the branched iPP should be one order smaller than for the linear iPP. For the linear iPP regime II occurs for a shear rate of 0.01 s^{-1} and thus this is expected to occur for shear rates typically of the order of 0.001 s^{-1} in the branched iPP. Similarly, regime II for the linear iPP starts at 3 s^{-1} and thus for the branched iPP regime III is expected to start at 0.3 s^{-1}. According to this all the results for the branched iPP should be in regime III. However, using the definition of the crystallization half time results the same distinct two regimes as for the linear polymer are, surprisingly, found for the branched material. The results for the branched polymer, as presented in Fig. 5, should, therefore, not be analyzed in terms of the classification scheme with application of the half-time.

We will try now to find a more appropriate way to distinguish between the different regimes, but we will first compare the results obtained from rheology and those obtained from WAXS. Time-resolved WAXS patterns at the beginning of the crystallization process for different flow conditions are observed in Fig. 7 for the linear iPP sample. In the quiescent state, WAXS patterns exhibited the typical isotropic crystal diffraction rings in (a). The anisotropy is clearly observed when the experiments are performed under shear conditions. When a shear strain of $\gamma = 60$ is applied, some orientation is observed but it is not very well developed, as it can be seen from the image in (b). In any case the shear rate applied is well inside the regime III ($\dot{\gamma} > 1/\tau_R^{HMW}$). At higher shear strain ($\gamma = 180$) the pattern is highly anisotropic, indicating large number of oriented crystals.

Khanna [10] has shown that rheological characterization is a useful complementary tool to track the crystallization of polymers from the melt. In that work a general relationship for the transformed fraction, $\alpha(t)$, as a function of the rheological results was proposed:

$$\alpha(t) = \frac{G'(t) - G'_0}{G'_\infty - G'_0} \tag{5}$$

where G'_0, $G'(t)$, and G'_∞ are the storage moduli at time 0, t, and infinity. We have analyzed the results presented in Figs. 4 and 5 to calculate $\alpha(t)$. The value for G'_0 has been taken as G' in the melt state prior to crystallization in quiescent conditions, the value for G'_∞ has been obtained by fitting the experimental results in Figs. 4 and 5 to a sigmoid dependence of viscoelastic properties with the crystallization time. The results are included in Fig. 8 for the branched iPP only to avoid data overcrowding. What is clearly seen is a good match of time scales in both rheological and WAXS experiments for the onset of the crystallization process. A correlation between the fractional change of viscoelastic properties and crystal content is observed. However, this correlation is not unique and depends on the pre-shear conditions applied. This is shown in Fig. 9. As the flow conditions are stronger for a given material, the G' values decrease for the same degree of crystal fraction. This means that the viscoelastic properties, and their evolution during the crystallization process do not only depend on crystal volume fraction at a given time, but also on the viscoelastic "nature" and the coupling between the different ordered and disordered developing phases. It is worth to remind that the viscoelastic properties in semicrystalline heterogeneous systems are the result of a very complex coupling between the existing different phases. On one hand, we have the disordered melt phase, which is transforming to a solid phase. On the other hand, this solid phase is not formed only by ordered structures, but also by disordered solid material unable to crystallize.

Although the exact relation between the space filling and the modulus is unknown, one can still measure how changes in space filling take place by considering the Avrami analysis. The Avrami model can be used to obtain quantitative information about crystal growth geometry:

$$1 - X_c(t) = e^{-kt^n} \tag{6}$$

where $X_c(t) = \alpha(t)X_{c,max}$, and k and n are the two Avrami parameters referred as the crystallization constant and the Avrami exponent. The exponent n depends on the nucleation type and growth geometry. For a thermal, heterogeneous nucleation $n = 3$ and a sphere-like crystal growth geometry is expected; for the same type of nucleation and $n = 2$ a disk-like growth it is expected, and $n = 1$ corresponds to linear crystal growth. In case of sporadic homogeneous nucleation and spherulitical growth $n = 4$ is found. The Avrami plots from transformed rheological properties are shown in Fig. 9. Other authors have recently tested the ability of the Avrami equation to describe the evolution of the linear viscoelastic properties in quiescent crystallization of polyethylene [28]. The exponent found for quiescent and flow-induced crystallization for the lowest shear rate pre-shear conditions is initially about 3 and that changes to a slope of 4 or even higher. This is probably due to Eq. 5 used for estimating $\alpha(t)$. The problem is that this relationship between the crystalline fraction and mechanical data is too simple to relate structure and morphology to rheological properties; a non-unique expression, different from expression 5, should be used (see for example Boutahar et al. [9]). However, what it is clear from Fig. 10 is that a sudden change in the exponent, and thus in the kinetic process, is observed when strong pre-shear conditions are applied, suggesting a change in the morphology of the growing crystalline structure from a spherulitical to a rod-like crystal morphology. Obviously more research is required for using, for example, optical and scattering techniques in line with the rheological testing. In this way a direct relationship between the growing structure and the development of rheological properties during the crystallization process can be reached. As a first step in this comparison, the Avrami equation has been also applied to the values of crystallinity obtained in WAXS experiments conducted in the same conditions than those showed in Fig. 10a. The results obtained are shown in Fig. 10b showing an excellent qualitative and even quantitative agreement with the results obtained from WAXS measurements. In what the branched sample concerns it is worth to comment that the analysis of the data using Avrami equation indicates that a large amount of nuclei for crystallization are more likely formed in this iPP sample, consistently with patent literature.

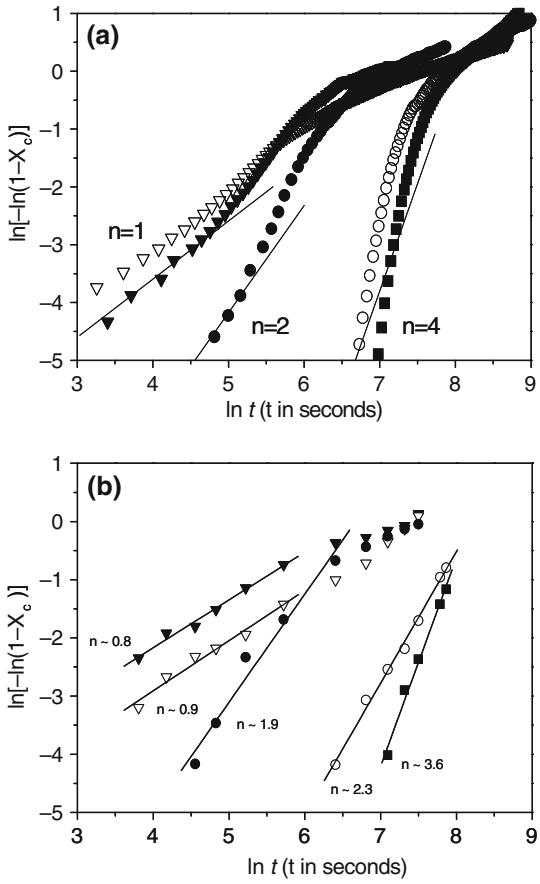

Fig. 10 **a** Avrami analysis of the results obtained from the storage modulus during crystallization at 418 K for the linear (*open symbols*) and the branched (*solid symbols*) samples for different conditions. **b** Avrami analysis of the results obtained from the 2D-WAXS measurements during crystallization at 418 K for linear (*open symbols*) and for the branched iPP (*solid symbols*) samples for different conditions. The symbols are the same as than in Fig. 9

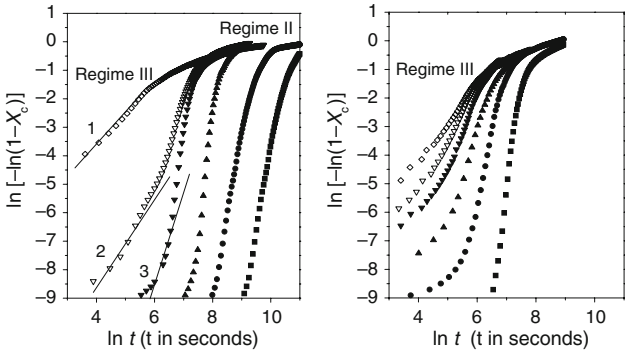

Fig. 11 Avrami analysis of the results obtained from the storage modulus during crystallization at 418 K for the linear (**a**) and the branched (**b**) samples for different conditions. The symbols in the figures correspond to: (*filled square*) quiescent, (*filled circle*) 4 s^{-1}/15 s, (*filled triangle*) 40 s^{-1}/1.5 s; (*filled inverted triangle*) 60 s^{-1}/1 s; (*open inverted triangle*) 60 s^{-1}/2 s and (*open diamond*) 60 s^{-1}/3 s

But what it is more interesting is that Avrami plots could be even much more appropriate way to study the different FIC regimes. For the linear polymer in left side of the Fig. 11 regime II is clearly observed by the horizontal shift of the curves. Regime III sets for a sufficient high shear rate and sufficient large shear time. Next to the shift, a change of the initial slope sets in. For the branched polymer Regime III is immediately observed by the change of the (initial) slope to a value of one. So the Avrami plots not only show the enhanced crystallization but also the change of regime and thus Avrami plots seem to be, for the polymers/cases we are considering, the most appropriate for the classification. They should, however, be treated with caution if one is looking at space filling and/or crystallinity.

Conclusions

The influence of molecular architecture and shear flow on the crystallization behavior of iPP was studied using a linear and a branched polymer. Rheological properties, which are strongly affected by the molecular architecture, are a key issue when studying FIC since they determine the different regimes that can occur. Long chain branching in iPP leads to enhanced shear thinning and elastic properties in shear, elongation thickening, and also a broader relaxation time spectrum. These properties have already for a long time been associated to the presence of this kind of structures in polyolefins. Flow strongly affects crystallization. At low and moderate pre-shear conditions lower values of the induction time for the onset of the crystallization process monitored by rheology are found. The effect is much more pronounced for long chain branched iPP than in linear iPP. However, for the latter a clear change in flow-enhanced crystallization kinetics is observed that is connected with two different regimes. These regimes are defined by two characteristic Deborah numbers that are defined by the characteristic reptation ($De_0 = \tau_R^{HMW}\dot{\gamma}$) and Rouse ($De_s = \tau_R^{HMW}\dot{\gamma}$) relaxation times for the high-M_w tail of the distribution. For conditions that fulfill $De_s = \tau_R^{HMW}\dot{\gamma} > 1$ (in the fibrillar regime), it is necessary to reach a characteristic shear strain (shear time) for a change in the crystallization kinetics. However, while in the branched iPP and increasing shear rate the change is smooth, a sudden change is observed for the linear one when a critical value of the shear strain (shear time) is reached.

What it is more interesting is the connection between the crystallization kinetics parameters obtained from rheological and WAXD measurements. Although the correct relationship between ongoing polymer structure and rheological properties has not been fully resolved, very similar kinetics is observed from both kinds of experiments. In fact, the match between the results obtained is not only

qualitative but also almost quantitative far from the expectations. Avrami plot applied to the fractional change of the rheological properties during crystallization have resulted in a very interesting tool to identify not only the crystallization regime, but also the different crystallization kinetics and hence the growing morphology.

References

1. Mendelson RA, Bowles WA, Finger FLJ. Effect of molecular structure on polyethylene melt rheology. I. Low-shear behavior. J Polym Sci Part A-2 Polym Phys. 1970;8:105–26.
2. Wild L, Ranganath R, Ryle T. Structural evaluation of branched polyethylene by combined use of GPC and gradient-elution fractionation. J Polym Sci Part A-2 Polym Phys. 1971;9:2137–50.
3. Vega JF, Santamaria A, Muñoz-Escalona A, Lafuente P. Small-amplitude oscillatory shear flow measurements as a tool to detect very low amounts of long chain branching in polyethylenes. Macromolecules. 1998;31:3639–47.
4. Malmberg A, Kokko E, Lehmus P, Löfgren B, Seppäla JV. Long-chain branched polyethene polymerized by metallocene catalysts $Et[Ind]_2ZrCl_2/MAO^{\dagger}$ and $Et[IndH_4]_2ZrCl_2/MAO$. Macromolecules. 1998;31:8448–54.
5. Malmberg A, Liimatta J, Lehtinen A, Löfgren B. Characteristics of long chain branching in ethene polymerization with single site catalysts. Macromolecules. 1999;32:6687–96.
6. Bin Wadud SE, Baird DG. Shear and extensional rheology of sparsely branched metallocene-catalyzed polyethylenes. J Rheol. 2000;44:1151–67.
7. Kolodka E, Wang WJ, Zhu S, Hamielec AE. Copolymerization of propylene with poly(ethylene-*co*-propylene) macromonomer and branch chain-length dependence of rheological properties. Macromolecules. 2002;35:10062–70.
8. Agarwal PK, Somani RH, Weng W, Mehta A, Yang L, Ran S, et al. Shear-induced crystallization in novel long chain branched polypropylenes by in situ rheo-SAXS and -WAXD. Macromolecules. 2003;36:5226–35.
9. Boutahar K, Carrot C, Guillet J. Crystallization of polyolefins from rheological measurements relation between the transformed fraction and the dynamic moduli. Macromolecules. 1998;31:1921–9.
10. Khanna IP. Rheological mechanism and overview of nucleated crystallization kinetics. Macromolecules. 1993;26:3639–43.
11. Langston JA, Colby RH, Chung TCM, Shimizu F, Suzuki T, Aoki M. Synthesis and characterization of long chain branched isotactic polypropylene via metallocene catalyst and T-reagent. Macromolecules. 2007;40:2712–20.
12. Macosko CW. Rheology: principles, measurements and applications. Minneapolis: Willey-VCH Publishers; 1994.
13. Steenbakkers RJA, Peters GWM. Suspension-based rheological modeling of crystallizing polymer melts. Rheol Acta. 2008;47:643–65.
14. van Meerveld J, Peters GWM, Hütter M. Towards a rheological classification of flow induced crystallization experiments of polymer melts. Rheol Acta. 2004;44:119–34.
15. Ogino Y, Fukushima H, Takahashi N, Matsuba G, Nishida K, Kanaya T. Crystallization of isotactic polypropylene under shear flow observed in a wide spatial scale. Macromolecules. 2006;39:7617–25.
16. Acierno S, Palomba B, Winter HH, Grizzuti N. Effect of molecular weight on the flow-induced crystallization of isotactic poly(1-butene). Rheol Acta. 2003;42:243–50.
17. van der Beek MHE. Specific volume of polymers: influence of the thermomechanical history. Ph.D. Thesis, Chapter 5. Eindhoven University of Technology, The Netherlands; 2005.
18. Doi M, Edwards SF. The theory of polymer dynamics. Oxford: Clarendon Press; 1986.
19. Vega JF, Rastogi S, Peters GWM, Meier HEH. Rheology and reptation of linear polymers. Ultrahigh molecular weight chain dynamics in the melt. J Rheol. 2004;48:663–78.
20. McLeish TCB, Milner ST. Entangled dynamics and melt flow of branched polymers. Adv Polym Sci. 1999;143:195–256.
21. Ketzmerick R, Öttinger HC. Simulation of a non-Markovian process modelling contour length fluctuation in the Doi-Edwards model. Continuum Mech Thermodyn. 1989;1:113–24.
22. Fetters LJ, Lohse DJ, Richter D, Witten TA, Zirkel A. Connection between polymer molecular weight, density, chain dimensions, and melt viscoelastic properties. Macromolecules. 1994;27:4639–47.
23. Fetters LJ, Lohse DJ, Graessley WW. Chain dimensions and entanglement spacings in dense macromolecular systems. J Polym Sci Part B Polym Phys. 1999;37:1023–33.
24. Peters GWM, Swartjes FHM, Meijer HEH. The influence of flow-induced crystallization on the impact toughness of high-density polyethylene. Macromol Symp. 2002;185:277–92.
25. Swartjes FHM, Peters GWM, Rastogi S, Meijer HEH. Stress induced crystallization in elongational flow. Int Polym Process. 2003;18:53–66.
26. Zuidema H, Peters GWM, Meijer HEH. Development and validation of a recoverable strain-based model for flow-induced crystallization of polymers. Macromol Theory Simul. 2001;10:447–60.
27. Seki M, Thurman DW, Oberhauser JP, Kornfield JA. Shear-Mediated Crystallization of Isotactic Polypropylene: The Role of Long Chain−Long Chain Overlap. Macromolecules. 2002;35:2583–94.
28. Bustos F, Cassagnau P, Fulchiron R. Effect of molecular architecture on quiescent and shear-induced crystallization of polyethylene. J Polym Sci Part B Polym Phys. 2006;44:1597–607.